Appl Phys A (2011) 105:529–546
DOI 10.1007/s00339-011-6595-6

Applied Physics A
Materials Science & Processing

The effect of the target structure and composition on the ejection and transport of polymer molecules and carbon nanotubes in matrix-assisted pulsed laser evaporation

Leonid V. Zhigilei · Alexey N. Volkov · Elodie Leveugle · Marshall Tabetah

Received: 2 July 2011 / Accepted: 20 August 2011 / Published online: 4 October 2011

Abstract Matrix-assisted pulsed laser evaporation (MAPLE) is a prominent member of a broad and expanding class of laser-driven deposition techniques where a matrix of volatile molecules absorbs laser irradiation and provides the driving force for the ejection and transport of the material to be deposited. The mechanisms of MAPLE are investigated in coarse-grained molecular dynamic simulations focused on establishing the physical regimes and limits of the molecular transfer from targets with different structures and compositions. The systems considered in the simulations include dilute solutions of polymer molecules and individual carbon nanotubes (CNTs), as well as continuous networks of carbon nanotubes impregnated with solvent. The polymer molecules and nanotubes are found to be ejected only in the ablation regime and are incorporated into matrix-polymer droplets generated in the process of the explosive disintegration of the overheated matrix. The ejection and deposition of droplets explain the experimental observations of complex surface morphologies in films deposited by MAPLE. In simulations performed for MAPLE targets loaded with CNTs, the ejection of individual nanotubes, CNT bundles, and tangles with sizes comparable or even exceeding the laser penetration depth is observed. The ejected CNTs align along the flow direction in the matrix plume and tend to agglomerate into bundles at the initial stage of the ablation plume expansion. In a large-scale simulation performed for a target containing a network of interconnected CNT bundles, a large tangle of CNT bundles with the total mass of 50 MDa is separated from the continuous network and entrained with the matrix plume. No significant splitting and thinning of CNT bundles in the ejection process is observed in the simulations, suggesting that fragile structural elements or molecular agglomerates with complex secondary structures may be transferred and deposited to the substrate with the MAPLE technique.

L.V. Zhigilei (✉) · A.N. Volkov · E. Leveugle · M. Tabetah
Department of Materials Science and Engineering, University of Virginia, 395 McCormick Road, Charlottesville, VA 22904-4745, USA
e-mail: lz2n@virginia.edu

1 Introduction and background

The ability of pulsed laser irradiation to remove (ablate) material from a target and deposit thin films of various organic and inorganic materials was demonstrated shortly after the invention of lasers [1]. Since then, pulsed laser deposition (PLD) has become an established method for producing thin films for a broad range of applications [2]. While application of PLD for the growth of both inorganic and organic/polymeric films has been active over the years, PLD of polymer films has been limited by unavoidable pyrolytic and/or photolytic fragmentation of polymer chains in the ablation process. Indeed, most of the models for laser ablation of polymer targets stipulate the chemical bond scission and the release of a substantial amount of volatile products of photochemical/photothermal reactions as a condition for the ablation onset [3–6]. Although for a limited number of addition polymers repolymerization can lead to a partial reconstruction of the original polymeric material after the deposition [7, 8], in most cases a substantial modification of the original target material is observed.

In order to enable application of the laser deposition technique in areas where preservation of the original structure and functionality of the deposited molecules is critical, a modification of PLD, dubbed matrix-assisted pulsed laser evaporation (MAPLE), has been developed [9–12]. The main distinctive feature of MAPLE is the use of a frozen dilute solution of the material to be deposited as a target in

the laser deposition setup. By choosing a relatively volatile solvent (or matrix) with strong absorption at the laser wavelength used in the deposition, it is possible to ensure the ejection, transport, and deposition of the solute molecules to the substrate through the entrainment in the expanding ablation plume of the matrix molecules. The preferential absorption of the laser light by matrix molecules and the relatively low temperatures required for the explosive boiling and ablation of the volatile matrix minimize or completely eliminate the photothermal and photochemical decomposition of the polymer molecules.

Since the initial demonstration of successful deposition of thin films for biosensor fabrication [9–11], the area of MAPLE applications has been steadily expanding and now includes deposition of thin films for polymer-based electronic and optoelectronic devices [13–16], growth of active protein films [17–21] and fabrication of coatings for drug delivery and tissue engineering [22–24]. With a proper choice of matrix and irradiation conditions, MAPLE technique has been largely successful in avoiding chemical modification of polymer molecules, as demonstrated by mass spectrometry analysis of the deposited material, e.g. [22, 25]. The fabrication of smooth films with low surface roughness, required for some of the applications [14, 16, 26], however, presents a significant challenge. High-resolution scanning electron microscopy (SEM) and atomic force microscopy (AFM) imaging of the deposited films commonly reveals rough surface morphology that contain signatures of the deposition of molecular clusters or droplets with characteristic sizes ranging from tens of nanometers to microns, e.g. [14, 19, 25–39].

The observations of substantial surface roughness contradict the original picture of the ejection and transport of individual polymer molecules in MAPLE [9–12], ingrained in the name of the technique, matrix-assisted pulsed laser *evaporation*, and are indicative of more complex processes responsible for the molecular transfer in MAPLE. The results of recent molecular dynamics (MD) simulations [40] suggest an alternative scenario of the molecular transfer in MAPLE that is consistent with the experimental observation of complex morphology of the deposited films. The simulations predict that the ejection of polymer molecules is not possible in the regime of molecular evaporation from the surface and takes place only in the ablation regime, when an explosive disintegration of matrix overheated above the limit of its thermodynamic stability results in the collective ejection of a mixture of vapor-phase molecules, small molecular clusters, and larger droplets. In all simulations performed for different laser fluences and polymer concentrations, the polymer molecules are found to be always ejected as parts of large polymer-matrix clusters/droplets that are likely to retain a large fraction of their matrix content at the time of the deposition to the substrate. The entanglement of the polymer molecules facilitates the formation of intricate elongated viscous droplets that can be related to the complex morphologies observed in polymer films deposited by MAPLE. Moreover, the effect of molecular redistribution in the ejected polymer-matrix droplets [41] and the dynamic processes occurring upon landing of the droplets on the substrate [42] have been connected to the formation of characteristic polymer structures (wrinkled "deflated balloons" and "collapsed pipes," complex arrangements of interconnected polymer filaments, and elongated "nanofibers") observed in MAPLE experiments [29–35, 41, 42].

The maximum size of the ejected droplets scales with the laser penetration depth, and the notion of the prominent role of the droplet deposition in MAPLE is confirmed in recent experimental studies that reveal an increase in the roughness of the deposited films with increasing absorption depth in both resonant infrared (RIR) [33, 36] and ultraviolet (UV) [35] MAPLE depositions. A substantial increase in roughness of films deposited in UV MAPLE with increasing number of laser pulses [34] is also consistent with accumulation of compositional and morphological changes in the target irradiated by multiple laser pulses, predicted in MD simulations [40]. The computational results reveal that preferential evaporation of the volatile solvent results in the formation of a polymer-enriched surface region, whereas the corresponding increased viscosity of the concentrated polymer solution facilitates the formation of extended morphological features weakly bound to the surface of the target. One can expect that these surface features are readily ejected upon irradiation by subsequent laser pulses. The connection between the roughness of the deposited films and solubility of the polymer material in the matrix has also been considered [32, 33, 35, 43] and, while observed for some systems [32], is found to be less apparent in others [33, 35, 43] (given that solvent completely dissolves the polymer material).

Overall, the simulations and experiments suggest that the ejection of matrix-polymer droplets is unavoidable in MAPLE and is related to the nature of the ablation process—explosive decomposition of the overheated matrix into clusters, droplets, and vapor-phase matrix molecules [40, 41, 44, 45]. The size of the droplets and the corresponding roughness of the deposited films are largely defined by the laser absorption depth [33, 35, 36], polymer concentration [33], and thermodynamic properties of the matrix [35, 43]. To a certain extent, the morphology of the deposited films can also be affected by keeping the substrate at an elevated temperature during the deposition [25, 34, 37, 43, 46]. The surface roughness is observed to diminish as the substrate temperature approaches or exceeds the polymer glass transition temperature.

While the collective and explosive nature of the molecular ejection process in short pulse laser ablation is responsible for the ejection of molecular droplets and generation of rough morphology of the deposited films, it

also opens up opportunities for transferring larger objects, e.g. nanostructural elements or building blocks for fabrication of nanocomposite materials. MAPLE deposition of metal dioxide (TiO_2 and SnO_2) nanoparticles and nanorods [43, 47, 48] has been shown to produce uniform nanoparticle coverage of both flat and rough substrates, whereas co-deposition of polymer material and colloidal nanoparticles [15] or carbon nanotubes (CNTs) [23, 29, 46, 49] has been demonstrated to produce thin nanocomposite films. The low deposition rates of less than 0.05 nm/laser pulse, characteristic of MAPLE [12], allow for a fine control over the thickness of the growing film and, potentially, can be used for fabrication of structurally and functionally graded nanocomposite films and coatings. Moreover, the composition of the nanocomposite films produced by simultaneous deposition of polymer molecules and CNTs is not limited by the sharp increase in material viscosity at high ($\geq$5–6 wt.%) concentrations of CNTs that constrains the capabilities of alternative fabrication techniques. The MAPLE deposition, therefore, may provide a unique opportunity for fabrication of nanocomposite materials with compositions and uniformity of the dispersion of CNTs that are not accessible with other techniques. The analysis of the distribution of nanoparticles [15] and CNTs [29, 46] in the deposited films suggests that, similarly to the polymer molecules, these nanostructural units are transferred in droplets. The optimization of the MAPLE technique aimed at decreasing the roughness of the deposited films, therefore, is likely to also result in a more uniform dispersion of the nanostructured elements in MAPLE deposited nanocomposite films.

In this work, we use the results of coarse-grained MD simulations to reveal the connections between the composition of MAPLE targets and the mechanisms of material ejection and transport to the substrate. The computational model and parameters of the systems used in the simulations are described below, in Sect. 2. The effect of the polymer concentration on the parameters of the ejected clusters/droplets is discussed in Sect. 3 based on computational predictions for MAPLE targets with different polymer concentrations. The results of the simulations performed for MAPLE targets loaded with CNTs are reported in Sect. 4 and the ability of the MAPLE technique to transfer these large and relatively rigid nanostructural elements is analyzed for different distributions of CNTs in the target. The results are summarized in Sect. 5.

2 Computational model

The simulations of laser ablation of frozen polymer solutions [40] are performed with a coarse-grained MD model combining the breathing sphere model [50] for simulation of the molecular matrix and the bead-and-spring model [51] for representation of polymer molecules. The intermolecular (non-chemical) interactions among the matrix and polymer molecules are described by an interatomic potential chosen to reproduce the van der Waals interactions in a typical molecular solid [52]. In the bead-and-spring model, the "beads" representing functional groups of a polymer molecule (monomers) are connected by anharmonic springs with strengths appropriate for a carbon–carbon bond in a polymer molecule. The intramolecular "springs" in the bead-and-spring model and the intermolecular interactions are described by potentials that are defined as functions of the distances between the surfaces of the spherical particles representing the matrix molecules ("breathing spheres") and polymer units. The radii of the breathing spheres are dynamic variables for which equations of motion are solved during the simulations. The internal degrees of freedom associated with the radial motions of the molecules are used for simulation of molecular excitation by photon absorption and vibrational relaxation of the excited molecules. The radii of "beads" in the polymer bead-and-spring model, on the other hand, are kept fixed during the simulations and the absorption of laser irradiation by polymer molecules is neglected. A detailed description of the model, as well as the functional form and the parameters of the interaction potentials describing the intermolecular interactions and the chemical bonding within the polymer chains are given in [40]. The parameterization of the potentials describing the matrix-polymer system is loosely based on experimental characteristics of poly(methyl methacrylate) (PMMA) solution in toluene.

To enable the investigation of the mechanisms of the ejection and transfer of CNTs in MAPLE, the coarse-grained model for the matrix-polymer system has been integrated with a mesoscopic dynamic model recently developed for CNTs [53–55]. The model represents each individual CNT as a sequence of stretchable cylindrical segments. The dynamic behavior of CNTs is governed by a mesoscopic force field that accounts for the internal stretching, bending, and buckling of nanotubes as well as for the van der Waals interactions among the CNTs. The harmonic parts of the stretching and bending potentials are parameterized for single-walled CNTs [53] based on the results of atomistic simulations performed with the reactive empirical bond-order (REBO) potential [56]. The transition to the anharmonic regime (nonlinear stress-strain dependence), fracture of CNTs under tension, and bending buckling behavior [55] are accounted for in the model. The intertube interactions are calculated based on the tubular potential method [54, 57] that allows for a computationally efficient and accurate representation of van der Waals interactions between CNT segments of arbitrary lengths and orientation. The tubular potential is parameterized to match the atomistic representation of the intertube interactions (summation over pairs of

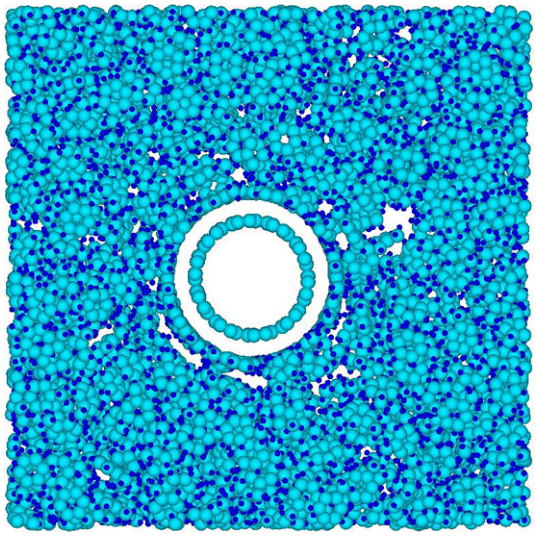

Fig. 1 Atomic configuration used in an atomistic simulation of a system containing 1020 toluene molecules and one (10,10) CNT. The carbon and hydrogen atoms are shown by *light* and *dark blue* spheres, respectively. The results of the atomistic simulations are used in parameterization of the mesoscopic model

interacting carbon atoms) as described within the adaptive intermolecular REBO (AIREBO) potential [58].

The interaction between the CNTs and matrix molecules is represented by the Lennard-Jones potential, $U(r_{ij}^s) = 4\varepsilon[(\sigma/r_{ij}^s)^{12} - (\sigma/r_{ij}^s)^6]$, defined as a function of the distance $r_{ij}^s = r_{ij} - R_M^i - R_T$ between the surfaces of a breathing sphere molecule i of an instantaneous radius R_M^i and a CNT j of a radius R_T, with r_{ij} being the distance between the center of the breathing sphere molecule and the axis of the nanotube. The nanotube ends are covered by semi-spherical caps which prevent molecules from getting inside the CNTs. The computational approach used in the calculation of the interaction between a molecule and a curved CNT is described in Ref. [59]. The parameters of the potential, $\varepsilon = 0.254$ eV and $\sigma = 3$ Å, are chosen based on the results of atomistic simulations of a toluene—CNT system performed with the AIREBO potential [58].[1] The simulations are carried out for an individual toluene molecule interacting with a single-walled (10,10) CNT, as well as for the same nanotube embedded into liquid toluene at a density close to the experimental density at room temperature, 0.867 g/cm^3 [60]. In the latter case, the computational cell consists of 1020 toluene molecules surrounding a 1000-atom segment of a nanotube, Fig. 1, and has dimensions of $6.0 \times 6.0 \times 6.1$ nm^3. The periodic boundary conditions are applied in all three directions.

[1]The force and energy subroutines implementing the AIREBO potential [58] are obtained courtesy of Prof. Steven Stuart of Clemson University and are implemented in a general purpose MD code.

Due to asymmetric shapes of toluene molecules, the interaction energy and the CNT-toluene equilibrium distance are very sensitive to the molecular orientation with respect to the nanotube. Depending on the orientation of a molecule, the equilibrium distance between the center of mass of the molecule and the surface of the nanotube varies from 3.4 to 5.8 Å, with the lowest energy configuration being the one where the plane of the aromatic ring is parallel to the axis of the nanotube and perpendicular to the normal from the center of the molecule to the axis of the CNT. This molecular orientation is also found to be characteristic of the first solvation shell formed around the CNT embedded into liquid toluene, as can be seen from Fig. 1. The energy of the interaction between the CNT and the surrounding molecules is found to be about -0.54 eV/Å, which is comparable to the value of -0.68 eV/Å determined in simulations of a similar system performed with a different interatomic potential [60].

For the system of a CNT surrounded by matrix molecules, the mesoscopic model with the choice of parameters ε and σ listed above predicts the total CNT-matrix interaction energy of -0.56 eV/Å and the equilibrium distance between the surfaces of a breathing sphere and a CNT of 3.37 Å. With the equilibrium radius of a breathing sphere of 1.4 Å, the corresponding distance between the center of the breathing sphere and the surface of the CNT is 4.77 Å. Since the interaction energy of two parallel (10,10) CNTs is about -0.1 eV/Å [54, 61], the interaction energy of a CNT with the matrix molecules is close to the one of a CNT with its six neighbors in a perfect CNT bundle. The solvation energy, defined as the total energy change associated with the introduction of a CNT into the matrix, is found to be -0.13 eV/Å. In addition to the CNT-molecules interaction energy, the solvation energy includes positive contributions from the surface energy of the cylindrical cavity in the liquid toluene required for accommodation of the CNT and the extra energy due to the structural rearrangement of molecules in the immediate vicinity of the nanotube. The negative value of the solvation energy does not necessarily imply that the CNTs are soluble in the matrix. Indeed, although the solvation energy is negative in the atomistic model of the toluene-CNT system, a substantial decrease in the configurational entropy of mixing results in a small but positive Gibbs free energy of solvation [60].

We would like to note that the accuracy of the parameterization of the mesoscopic model is limited by the simplicity of the representation of matrix molecules by spherical particles. The atomistic simulations of CNT-toluene system are used here only as a general guidance in designing a model that captures the essential characteristics of matrix-CNT interactions. While the distribution of nanotubes in frozen MAPLE target is largely defined by the free energy of solvation and the sample preparation procedures, one can

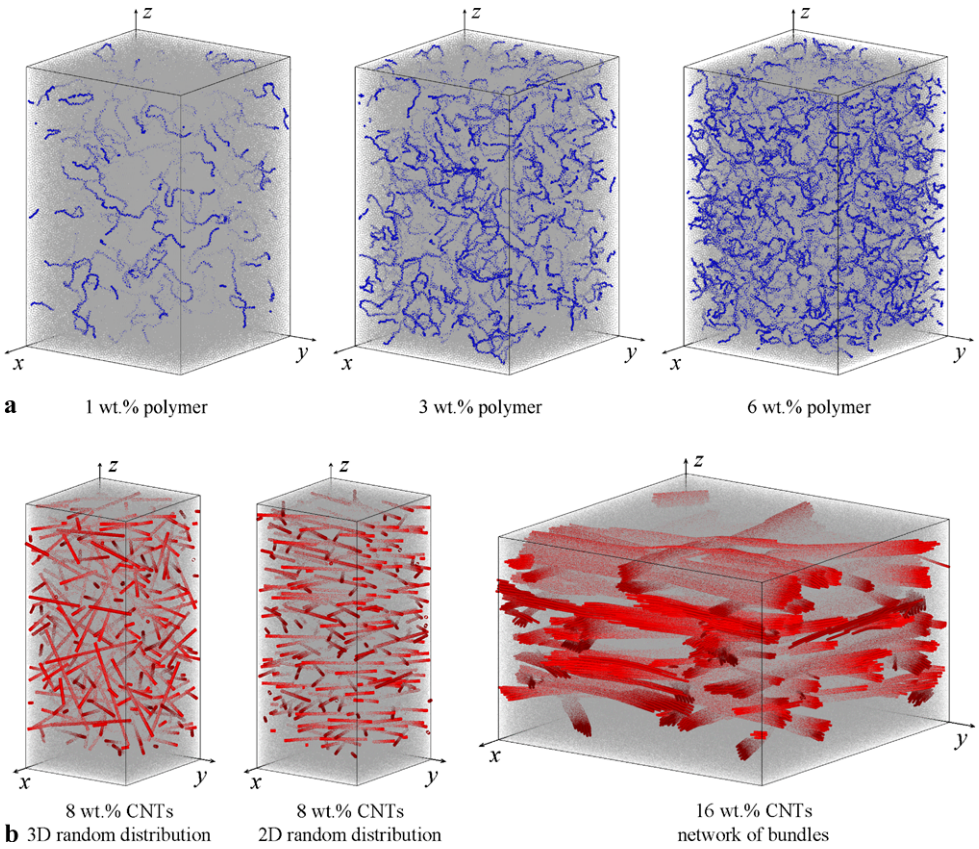

Fig. 2 The initial computational systems used in simulations of MAPLE. MAPLE targets contain 1 to 6 wt.% of polymer chains (**a**) and 1 to 17 wt.% of CNTs (**b**). The units of polymer chains are shown as *blue particles*, the nanotubes are shown as *red cylinders*, and the matrix molecules are shown as small *gray dots*. The periodic boundary conditions are applied in x and y directions, a pressure-transmitting boundary condition is applied at the *bottom* of the computational cells, and laser pulse is directed from the *top*, against the z-axis

expect that, for a given structure and composition of the target, the characteristics of the ablation process are much less sensitive to the variations of the thermodynamic parameters of the solution. Therefore, in this work, we explore the effect of the CNT solubility by considering different initial distributions of CNTs in the matrix, from a random distribution of individual nanotubes to an interconnected network of bundles, while keeping the parameters of the CNT-matrix interaction potential fixed.

Since all three components of the mesoscopic model (the breathing sphere model for matrix molecules, the bead-and-spring model for polymer chains, and the mesoscopic model for CNTs) adopt coarse-grained representations of the molecules and nanotubes, the sizes of computational cells in dynamic simulations can be sufficiently large to reproduce the collective processes leading to the molecular ejection in MAPLE. The systems used in the simulations of MAPLE are illustrated in Fig. 2. In all simulations, the periodic boundary conditions are applied in the lateral (parallel to the surface of the target) directions and a pressure-transmitting boundary condition [62] is applied at the bottom of the computational cells. In the simulations of laser ablation of polymer solutions, the computational cells have dimensions of $40 \times 40 \times 60$ nm^3 (676961 molecules for pure matrix) and polymer chains are randomly and uniformly distributed in the sample, Fig. 2a. The polymer concentrations of 1, 3, and 6 wt.% are used in the simulations and the corresponding numbers of polymer chains in the computational cells are 67, 202, and 381. Each matrix molecule and a monomer unit in a polymer molecule have the same molecular weight, 100 amu. This weight corresponds to the weight of a PMMA monomer and is close to the weight of molecules typically used as MAPLE matrices, e.g., toluene (92 Da), chloroform (118 Da), and glycerol (92 Da). Each polymer chain contains 100 monomer units and has a total molecular weight of 10 kDa.

In the simulations of MAPLE targets with CNTs, the concentration of nanotubes is varied from 1 to 17 wt.% and the length of the CNTs is varied from 16 to 150 nm. The length of the CNTs considered in the simulations is relatively small and is limited by the computational cost associated with modeling large computational cells consisting of millions of matrix molecules (see below). Experimentally, the short CNTs can be produced by chemically assisted cutting of CNT networks into short "fullerene pipes" that form stable suspensions in water in the presence of surfactants [63]. The results obtained in simulations of laser ablation of CNT solutions may also be relevant to recent observations of MAPLE deposition of 20–40 nm long TiO_2 nanorods [43] and other elongated structural units. The computational cells have a depth (size along the z-axis) of 109 nm and dimensions in the lateral (parallel to the irradiated surface, along

the x- and y-axes) directions that depend on the length of the CNTs. In particular, the lateral dimensions of 20×20 nm^2, 30×30 nm^2, 50×50 nm^2, and 169×169 nm^2 are used for CNTs with lengths of 16, 24, 44, and 150 nm, respectively. Three distinct types of structural arrangement of CNTs in the MAPLE targets are considered in the simulations. The first structure (to be referred to as *3D random*) is produced by placing randomly positioned and oriented individual CNTs within the computational cell, e.g., the left frame in Fig. 2b. The second structure (*2D random*) is generated by stacking thin layers of straight nanotubes that are randomly oriented within the layers, e.g., the middle frame in Fig. 2b. The third structure (*network of bundles*) is produced in dynamic mesoscopic simulations of a large number of interacting CNTs that are initially arranged into a 2D random structure [54, 55, 64]. The CNTs are found to spontaneously self-organize into continuous networks of bundles with partial hexagonal ordering of CNTs within the bundles and structural characteristics matching those of CNT mats, films, and buckypaper [63, 65, 66]. The formation of stable networks of bundles is observed only for CNTs that are longer than ~120 nm [55] and the nanotubes with length of 150 nm are used in this work to generate the network structure illustrated in the right frame of Fig. 2b.

The MAPLE targets are produced by inserting the CNT structures into the matrix, removing the matrix molecules overlapping with the CNTs and cooling the systems to zero temperature. Experimentally, the MAPLE targets with well-dispersed CNTs can be obtained through various methods, including sonication of CNT solutions and stabilization of dispersed solutions by covalent or non-covalent functionalization of the nanotubes, e.g. Refs. [67, 68]. The networks of bundles embedded into the solvent can be produced by filling a buckypaper structure with a matrix material in a process similar to the buckypaper impregnation method used for fabrication of CNT nanocomposites [69, 70]. The largest systems used in the simulations, such as the one shown in the right frame of Fig. 2b, are composed of ~ 20 millions of matrix molecules and more than a thousand of 150-nm long CNTs. To enable computational treatment of such systems, the model is implemented in a parallel code designed to ensure a good scalability for massively parallel simulations.

The laser irradiation is simulated by depositing quanta of energy equal to the photon energy (3.68 eV for wavelength of 337 nm) into the kinetic energy of the breathing mode of molecules chosen in a manner that ensures an exponential attenuation of the laser light with depth [40, 44]. Since the goal of this study is to elucidate the effect of the composition of MAPLE targets on the mechanisms of molecular ejection, the same laser pulse duration of 50 ps, optical penetration depth of 50 nm, and laser fluence of 8 mJ/cm^2 are used in all simulations. The absorption by polymer molecules and CNTs is neglected in the simulations. An estimation of the contribution of CNTs to the absorption of 1 to 17 wt.% CNT solutions based on the absorption cross-sections of CNTs [71] suggests that the strongly absorbing solvent makes the dominant contribution to the overall absorption of the solution (the effective penetration depth of the CNT part of 1 wt.% solution is estimated to be from 6.4 to 29.3 μm). The fluence of 8 mJ/cm^2 is about 2.3 times above the threshold fluence for the transition from the regime of molecular desorption (evaporation) from the surface to the explosive boiling of the overheated matrix and collective material ejection [40, 44, 45, 72]. The choice of the laser pulse duration and optical penetration depth ensures that the regime of thermal confinement [40, 44, 72, 73], characteristic of the majority of MAPLE experiments, is also realized in the simulations. In this irradiation regime, the pulse duration is shorter than the time of thermal diffusion across the absorption depth and the heat conduction does not contribute to the energy redistribution during the laser pulse. At the same time, the pulse duration is longer than the time required for the mechanical relaxation (expansion) of the absorption region and the conditions of the inertial stress confinement [40, 44, 72–75] are not realized in the simulations.

In order to compare the conditions leading to the molecular ejection in MAPLE to the ones in PLD, we also present the results obtained in a simulation of laser ablation of a pure polymer target at a laser fluence just above the threshold for the ablation onset. This simulation is performed with a model that is parameterized to represent a film composed of lysozyme molecules and deposited on a transparent substrate. The model will be described in detail elsewhere. Briefly, the lysozyme molecules are represented by the bead-and-spring model, the interaction potential is chosen to reproduce strong chemical bonding (3.48 eV) between the linked polymer units and weak non-bonded interactions (0.1 eV) between the molecules. The system used in the simulation consists of 360 lysozyme chains arranged in globular conformations. Each globule has 143 monomer units, with a mass of a unit being 100 Da. The size of the computational cell is $12.3 \times 12.3 \times 41$ nm^3, periodic boundary conditions are applied in the directions parallel to the irradiated surface, and the interaction with a rigid optically transparent substrate at the bottom of the computational cell is assumed to be 3 times stronger than the non-bonded intermolecular interactions. The laser wavelength of 355 nm, penetration depth of 30 μm, pulse duration of 350 ps, and fluence of 4 J/cm^2 are used in the simulation of the lysozyme system.

3 Laser ablation of polymer solutions: The effect of polymer concentration

A detailed analysis of the results of MD simulations of the ejection and transport of polymer molecules in MAPLE has

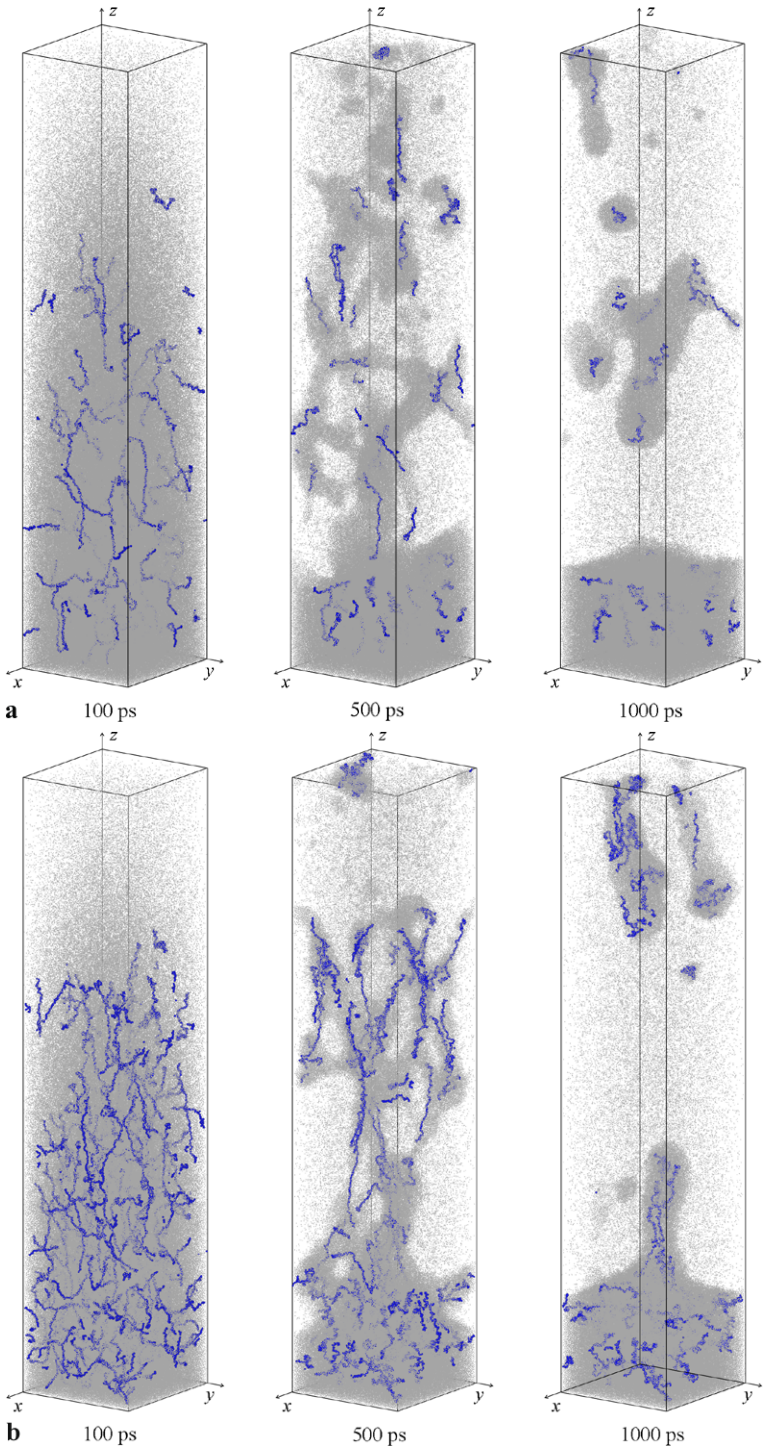

Fig. 3 Snapshots of molecular configurations obtained in simulations of MAPLE with polymer concentration in the target equal to 1 wt.% (**a**), 3 wt.% (**b**), and 6 wt.% (**c**). The units of polymer chains are shown as *blue particles* and the matrix molecules are shown as *small gray dots*. Animated sequences of snapshots from the simulations illustrated in (**a**) and (**c**) can be found at [76]

been presented in Ref. [40]. Here, some of the main conclusions of the earlier simulations are briefly reviewed and supported by additional data. The conditions leading to the ejection of intact polymer molecules in MAPLE are contrasted to the ones in ablation of polymer targets (relevant to PLD), where the extensive bond scission is observed close to the threshold for the ablation onset.

The processes leading to the molecular ejection in laser ablation of MAPLE targets with different polymer concentrations are illustrated by snapshots shown in Fig. 3 [76]. The laser fluence applied in the simulations exceeds the ablation threshold [40, 44, 77, 78] by more than a factor of two and the material ejection is driven by the explosive boiling of matrix overheated up to the limit of its thermodynamic sta-

Fig. 3 (*Continued*)

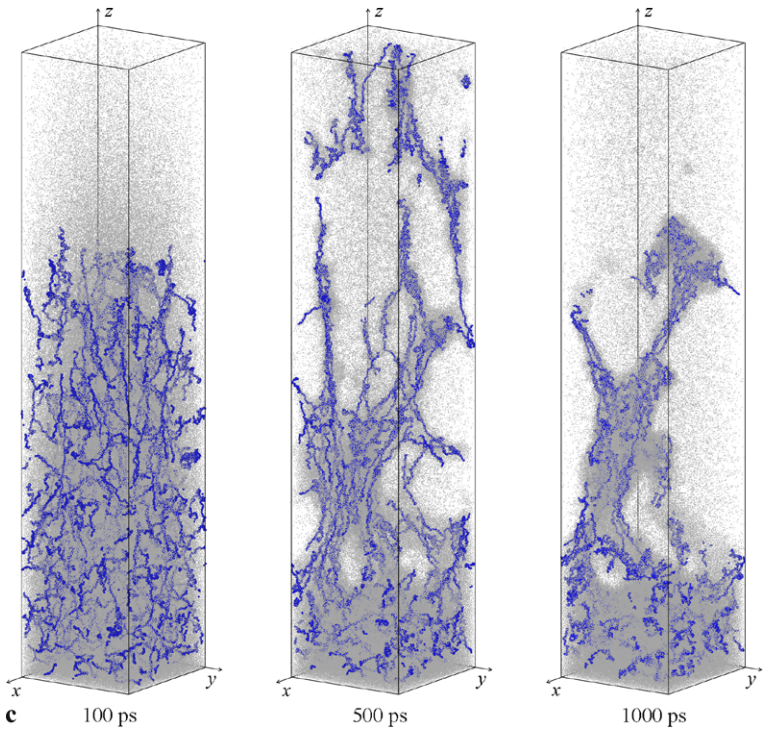

bility (∼90% of the critical temperature [40, 78–82]). The initial rapid expansion of the overheated part of the target (snapshots shown for 100 ps) is driven by the release of matrix vapor and results in the transformation of the overheated liquid into a two-phase mixture with intricate foamy structure of interconnected liquid regions surrounded by matrix vapor (snapshots shown for 500 ps). These transient foamy structures gradually decompose into separate liquid droplets surrounded by vapor-phase molecules as the expansion and cooling of the part of the target undergoing the explosive boiling continues (snapshots shown for 1000 ps).

An important conclusion one can draw from the simulations illustrated in Fig. 3, as well as from other simulations performed for various target materials [72, 82], is that the ejection of molecular clusters and liquid droplets is an unavoidable characteristic feature of the material ejection in the ablation regime. The explosive boiling of the overheated matrix does not result in complete vaporization of the ejected part of the target but leads to the generation of an ablation plume consisting of a mixture of vapor, molecular clusters, and liquid droplets. The degree of the overheating decreases with depth in the irradiated target, and the process of material decomposition at the initial stage of the ablation plume formation exhibits a strong dependence on the depth of origin of the ejected material [45]. The fraction of the vapor phase is the largest near the front of the expanding plume, small and medium-size clusters dominate in the middle of the plume, and large droplets form in the tail of the plume as a result of the decomposition of coarse liquid structures generated near the surface of the remaining target (see snapshots for 500 and 1000 ps in Fig. 3).

The complex dynamics of the plume formation results in a broad size distribution of the ejected clusters/droplets. The probability distribution functions of the number of ejected clusters are shown for the simulations of MAPLE with polymer concentrations of 1 and 6 wt.% in the top panels of Fig. 4. In the distributions, plotted in double-logarithmic scale and normalized to the number of individual matrix molecules, one can readily distinguish two distinct parts that correspond to small, up to ∼20 molecules, and large, up to tens of thousands molecules, clusters. Both parts of the distributions can be relatively well described by a power law $Y(N) \propto N^{-\tau}$, where N is the number of molecules or polymer units (mers) in the clusters and the exponent $-\tau$ is different for the low- and high-mass parts of the distributions. The decay of the probability to find clusters of increasingly larger size is substantially slower in the high-mass part of the distribution and the absolute value of the exponent is more than twice smaller compared to the one for the small clusters. The cluster size distributions are found to exhibit a relatively weak sensitivity to laser fluence (as soon as it is above the ablation threshold) and polymer concentration, with power law exponent $(-\tau)$ ranging from -4.1 to -3.5 for small clusters and from -1.6 to -1.1 for larger clusters in simulations performed for polymer concentrations from 0 to 6 wt.% and laser fluences from just above the ablation threshold to more than 2.5 the threshold [40]. Similar power law mass distributions of surface features have been evaluated based on analysis of SEM images of surface mor-

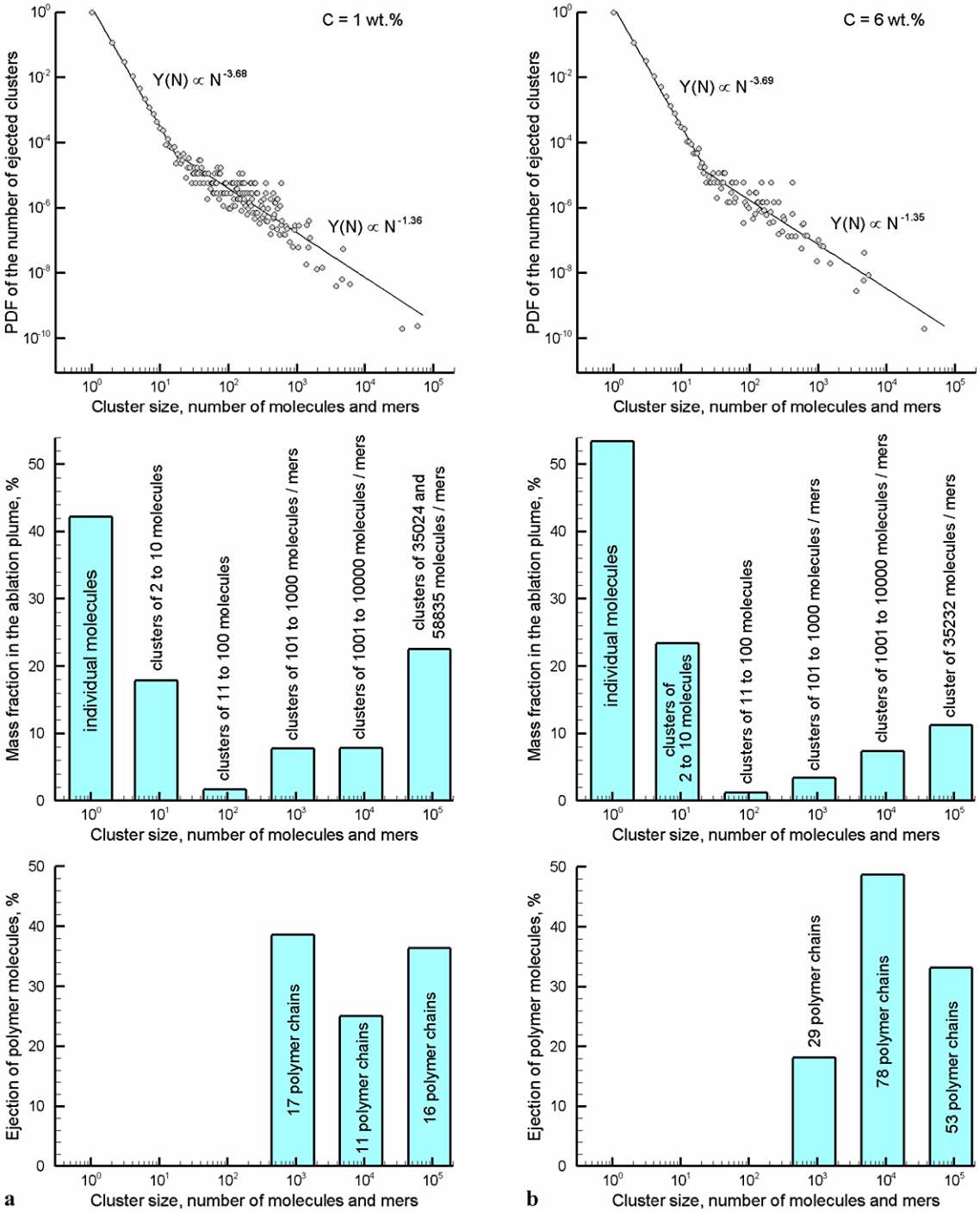

Fig. 4 Size distributions of matrix-polymer clusters in the plume ejected in simulations of MAPLE with polymer concentration of 1 wt.% (**a**) and 6 wt.% (**b**). The probability distribution functions (PDF) of the number of ejected clusters are shown in the *top* panels, mass percentages of the ejected clusters in the total ablation yield are shown in the *middle* panels, and the ejection of polymer chains with clusters of different sizes is shown in the *bottom* panels

phologies in polymer films deposited by MAPLE [83]. The experimental power law exponent of −1.65 is close to the ones predicted in the simulations for the high-mass parts of the distributions. The polymer concentration in large clusters exhibits a weak cluster size dependence and the mass of the polymer material deposited with matrix-polymer clusters can be expected to have distributions that are similar to the ones of matrix-polymer clusters/droplets.

One observation from the simulations that is of direct relevance to MAPLE film deposition is that the polymer

molecules are always ejected as parts of large matrix-polymer droplets or clusters. This is apparent from the histogram of the number of polymer chains ejected within clusters of different sizes shown in the bottom panels of Fig. 4. Although at both polymer concentrations the individual molecules and small clusters of several molecules account for the largest fraction of the total mass of the ejected plume (see middle panels of Fig. 4), most of the polymer molecules are ejected with large matrix droplets consisting of thousands of molecules. In particular, the two largest droplets ejected from the target with 1 wt.% polymer concentration and the largest droplet ejected from the target with 6 wt.% polymer concentration contain more than 30% of the total number of ejected polymer chains. Although the size of the matrix-polymer droplets decreases somewhat due to the evaporation of matrix molecules as the ablation plume expands, the evaporative cooling is found to quickly (within 1–2 ns after the formation of the droplets) stabilize the composition of the droplets. One can expect, therefore, that the droplets retain a large fraction of matrix material at the time of the deposition to a substrate and the growth of polymer films in MAPLE proceeds through the deposition of matrix-polymer clusters. These computational predictions are consistent with numerous experimental observations of surface morphologies that contain clear signatures of cluster deposition [14, 19, 25–39, 41, 42].

The effect of the polymer concentration in MAPLE targets on the parameters of the ejected clusters/droplets can be discussed based on the results shown in Fig. 4 for polymer concentrations of 1 and 6 wt.%. In the case of the smaller polymer concentration, a substantially larger fraction of polymer molecules is ejected with small clusters composed of less than 1000 matrix molecules and polymer units. Each of these clusters contains only one or two polymer chains surrounded by several tens to a few hundreds of matrix molecules. Several examples of such small clusters are shown in Fig. 5a. The fraction of polymer chains ejected in small clusters drops by about a factor of 2 when the polymer concentration in the target increases to 6 wt.%. In this case, the main contribution to the polymer yield is coming from larger clusters that contain from 2 to 23 polymer chains surrounded by thousands of matrix molecules, e.g. Fig. 5b, c.

The smaller fraction of matrix material ejected with the largest (more than 10000 molecules) clusters and the larger fraction of the individual molecules observed in the case of the larger polymer concentration (middle panels of Fig. 4) are related to the stabilizing effect of the entangled polymer molecules on the liquid structures generated near the surface of the target by the explosive boiling of the volatile matrix. The large liquid structure observed in the snapshot shown for 1000 ps in Fig. 3c is not able to separate from the target,

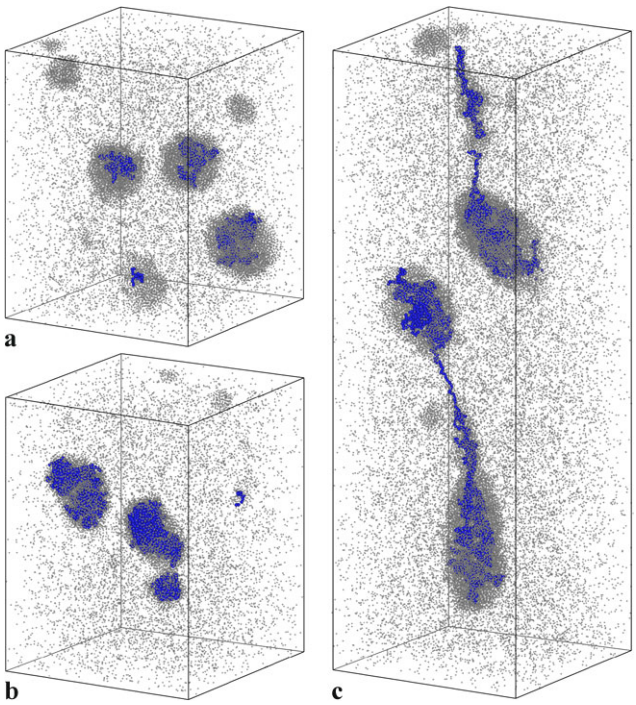

Fig. 5 Snapshots of several typical molecular clusters/droplets present in the plume ejected in MAPLE of polymer solutions. Snapshots are taken at 1 ns after the beginning of the laser pulse in simulations performed for targets with polymer concentration of 3 wt.% (**a**) and 6 wt.% (**b**), (**c**). The units of polymer chains are shown as *blue particles* and the matrix molecules are shown as *small gray dots*. Some of the clusters in the snapshots are split into two parts by the periodic boundary conditions, e.g. the small clusters that appear to contain fragments of polymer chains in the *lower part* of (**a**) and *right part* of (**b**) are actually parts of larger clusters shown at the opposite sides of the computational cells

leading to the decrease in the total ablation yield in this simulation (the total yield is ∼25% lower in the simulation performed with 6 wt.% polymer concentration compared to the one with 1 wt.%). The lower total yield is also reflected in the higher fraction of the individual molecules, even though the actual number of vapor-phase molecules is ∼5% lower in this simulation as compared to the one performed with 1 wt.% polymer concentration.

When relating the results of the simulations to experimental observations, it is important to note that the laser penetration depth of 50 nm, used in the simulations, is substantially shorter than the ones characteristic of the majority of MAPLE experiments. The pulse duration and laser penetration depth in the simulations is chosen to ensure the same physical conditions of thermal but not stress confinement as in MAPLE experiments performed with nanosecond laser pulses (see Sect. 2). The general physical picture of the simulated molecular ejection, therefore, can be expected to match the one in the experiments. The larger length-scale of the ablation phenomenon in MAPLE experiments, however, can be expected to result in the ejection of much larger

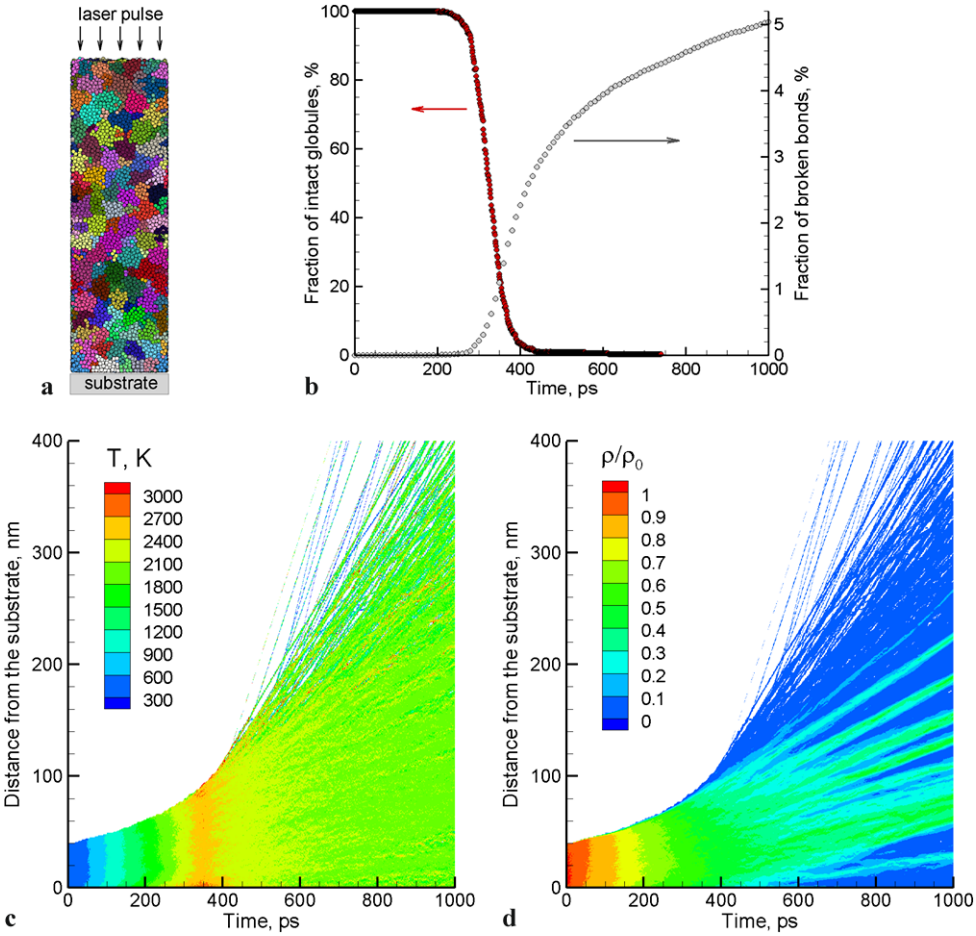

Fig. 6 The results of a simulation of laser ablation of a polymer film (without matrix) at a laser fluence close to the ablation threshold and laser pulse duration of 350 ps. The initial system representing a thin film composed of globular molecules and deposited on a transparent substrate is shown in (**a**), with individual molecules colored by different random color. The evolution of the fraction of broken chemical bonds and the number of intact polymer molecules is shown in (**b**). The contour plots of the temperature and density are shown in (**c**) and (**d**), respectively. Density scale is normalized to the initial density before the irradiation, ρ_0

molecular droplets, as the maximum size of the droplets is likely to scale with the laser penetration (and ablation) depth. Indeed, the increase in the roughness of the deposited films with increasing laser penetration depth has been observed in a number of MAPLE depositions [33, 35, 36].

With the account of the difference in the time- and length-scales between the simulations and experiments, the computational prediction of the increase in both the total number of the ejected polymer chains and the size of the polymer-matrix clusters with increasing polymer concentration in the target can be related to experimental observations of the linear increase of the thickness and roughness of the deposited films with increasing polymer concentration (up to 8 wt.%) reported in Ref. [33], as well as the improvement in the uniformity of the distribution of nanoparticles deposited in MAPLE with lower concentration of nanoparticles in the target [15]. The increase in the polymer concentration in the target is also found to facilitate the ejection of elongated droplets, e.g. Fig. 5c, and the generation of complex surface structures stabilized by the entanglement of polymer molecules, e.g. a snapshot for 1000 ps in Fig. 3c. The ejection of the elongated droplets may be related to the observations of extended "nanofiber" surface features in SEM images of PMMA films deposited by MAPLE [29, 30, 42, 83, 84], whereas the formation of polymer-rich surface structures can result in roughening and swelling of the surface region of the target and can make the ejection process to be sensitive to the number of laser pulses directed at the same area of the target [34].

An important conclusion from all of the MAPLE simulations is that intact polymer molecules can be ejected and deposited to the substrate. Not a single bond scission event is detected in any of the simulations. This observation is in a sharp contrast with ablation of polymer targets in PLD, where the dissociation of a large fraction of chemical bonds appears to be unavoidable [3–6]. To illustrate this point, the results obtained in a simulation of laser ablation of pure polymer (lysozyme) target at a laser fluence just above the threshold for the ablation onset are shown in Fig. 6. The computational system represents a thin polymer film deposited on a transparent substrate, Fig. 6a, and irradiated by a 350 ps laser pulse at a laser wavelength of 355 nm. The laser penetration depth of 30 μm, assumed in the simulation, is much larger than the thickness of the film, 41 nm. The laser energy deposition, therefore, results in the even heating throughout the thickness of the film during the laser

pulse, Fig. 6c. It is apparent from the time dependence of the fraction of broken bonds shown in Fig. 6b that active photothermal bond scission starts close to the end of the laser pulse, when the temperature of the film reaches ∼2500 K, Fig. 6c. The release of small volatile fragments generated in the pyrolytic decomposition of polymer molecules drives the ejection of the larger polymer fragments and molecular droplets. The ablation mechanism in this case has some similarity to MAPLE, with the volatile products of the thermochemical decomposition serving the role of matrix that drives the ejection process. One important difference, however, is that the thermodynamic parameters of the matrix material in MAPLE can be chosen so that no thermal decomposition of polymer molecules takes place at the threshold for the explosive boiling of the matrix, whereas in the case of pure polymer target the thermal decomposition is a required step of the ablation process and no ejection of intact polymer molecules can be expected, Fig. 6b.

4 Ejection and transport of CNTs in MAPLE

The ability of MAPLE technique to transfer and deposit single- and multi-walled CNTs has been demonstrated in a number of experiments [23, 29, 46, 49], where the CNTs are co-deposited with polymer material to form nanocomposite thin films. In this section, we report first simulations aimed at understanding of the physical mechanisms responsible for the ejection and transfer of CNTs in MAPLE. The simulations are performed for CNTs of different length (from 16 to 150 nm), and for targets with different CNT concentrations (from 1 to 17 wt.%) and structural arrangements of CNTs (*2D* and *3D random*, *network of bundles*, see Sect. 2).

The visual picture of the ejection of CNTs from MAPLE targets is shown in Fig. 7 for CNTs with length of 44 nm. Similarly to MAPLE of polymer molecules (Fig. 3), the explosive boiling of the overheated matrix and associated rapid release of the matrix vapor drives the rapid expansion of surface regions of the target. The CNTs are entrained into the expanding matrix plume and are lifted off from the target. One of the effects that are apparent from the snapshots shown in Fig. 7 is a clear tendency of the ejected nanotubes to align along the flow direction of the matrix plume (normal to the irradiated surface). The trend for CNTs to align along the flow direction is particularly strong in simulations where the CNTs are randomly oriented in the initial target (*3D random* arrangement), Fig. 7a, b, but is also present in the simulations where all CNTs are initially parallel to the surface (*2D random* arrangement), Fig. 7c. The alignment of CNTs is similar to that of polymer molecules, Fig. 3, and is related to the partial immersion of CNTs into liquid droplets in the presence of the high-velocity flow of the expanding matrix vapor.

The alignment is observed for nanotubes of different length and is an important factor that facilitates bundle formation in the plume. While in all three simulations illustrated in Fig. 7 the individual CNTs are randomly distributed in the target (perfect dispersion), the formation of small groups of parallel tubes agglomerating into bundles can be observed at the early stage of the plume expansion for targets with sufficiently high concentration of CNTs, Fig. 7b, c. The higher is the concentration of CNTs in the target and the shorter are the CNTs, the more active is the bundle formation during the ejection process. For example, a typical cluster of several aligned 44 nm long CNTs is shown in a snapshot of a MAPLE plume in Fig. 8a, and a more compact well-developed bundle with the hexagonal arrangement of ten 16 nm long CNTs embedded into a droplet of matrix molecules is shown in Fig. 8c.

Another characteristic type of matrix-CNT structure found in the plume is the tangle of CNTs surrounded by liquid matrix. Although the formation of complex liquid structures strung together by randomly arranged CNTs can be observed even for relatively short CNTs, e.g. Fig. 8b, the ejection of extended tangles of CNTs becomes more pronounced for targets with longer nanotubes. In particular, fast entanglement of 150 nm long CNTs and ejection of large clusters of interconnected CNTs attached to liquid matrix takes place in a large-scale simulation illustrated in Fig. 9a. The nanotubes in this case are randomly dispersed within 2D layers in the target and the formation of the tangles composed of interconnected bundles of CNTs is happening very quickly, during the first nanosecond of the ejection process. The observation of the active formation of bundles and tangles of nanotubes at the initial stage of the molecular ejection in MAPLE suggests that the ability to obtain well-dispersed distributions of CNTs in nanocomposite films deposited by MAPLE is likely to be limited by the strong tendency of nanotubes to agglomerate at the initial stage of the ejection process. Indeed, the initial experimental results [29, 46] support the computational prediction that CNTs are deposited in MAPLE as parts of large matrix-polymer-CNT clusters and entangled network fragments.

The agglomeration of CNTs in the matrix may result in the formation of bundles and CNT networks even before the laser irradiation. In particular, agglomeration of single-walled CNTs in toluene is noted during the MAPLE target preparation [46]. This leads to the question on the ability of MAPLE to disintegrate the CNT networks and transfer the individual CNTs or CNT bundles separated from the network structures to the substrate. To address this question, a large-scale simulation of MAPLE is performed for a target composed of a network of interconnected CNT bundles immersed into a frozen matrix solvent (see right frame of Fig. 2b). The initial dynamics of the disintegration of the

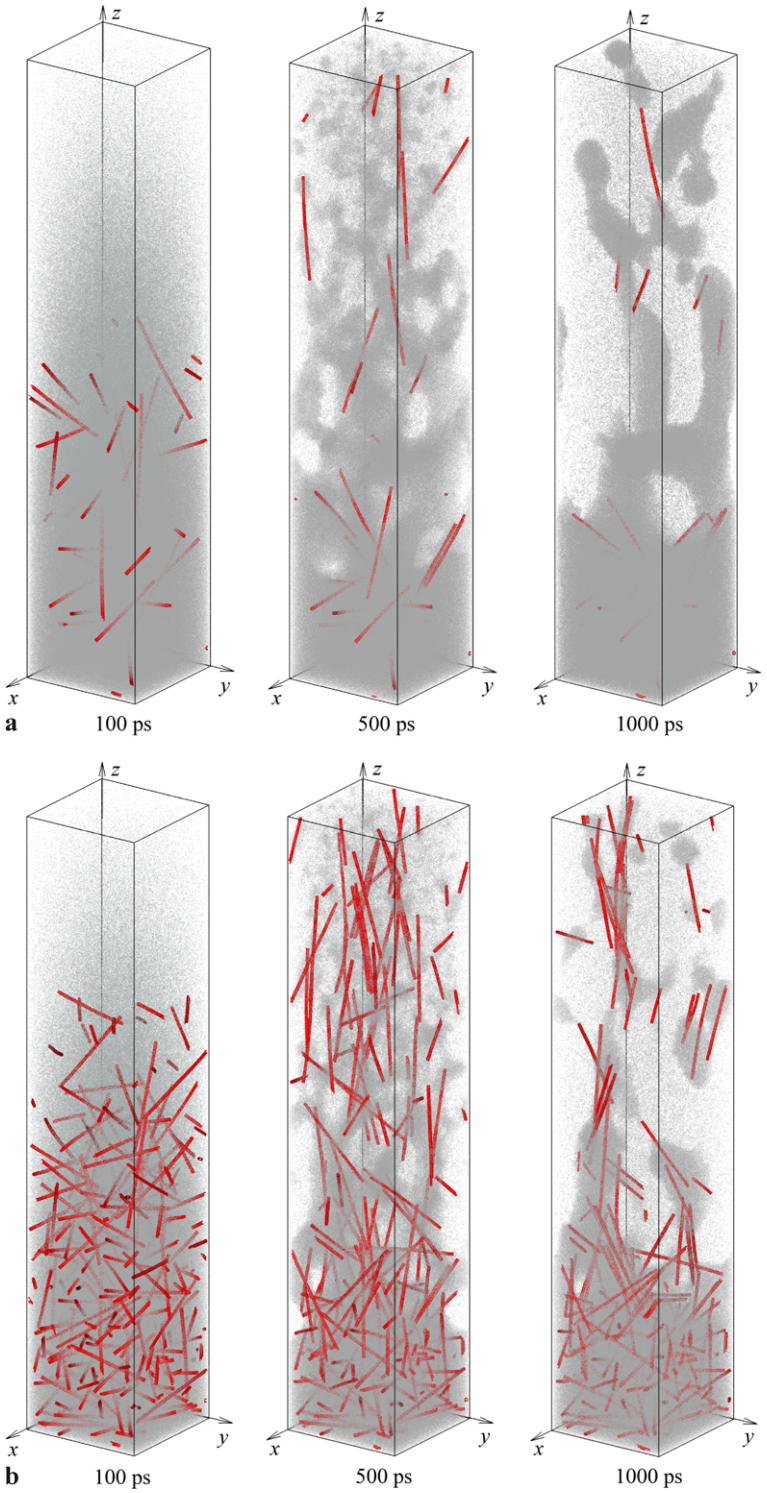

Fig. 7 Snapshots of molecular configurations obtained in simulations of the ejection of CNTs from MAPLE targets with different compositions and structures. The initial concentration of 44 nm long CNTs in the MAPLE targets is 1 wt.% in (**a**) and 8 wt.% in (**b**) and (**c**). The arrangement of the individual nanotubes in the targets is *3D random* in (**a**) and (**b**), and *2D random* in (**c**). The nanotubes are shown as *red cylinders* and the matrix molecules are shown as *small gray dots*. Animated sequence of snapshots from the simulation illustrated in (**c**) can be found at [76]

network structure driven by the explosive boiling of the matrix material is illustrated in snapshots show in Fig. 9b. Although there are no signs of any significant splitting or thinning of the thick bundles present in the network structure, the separation and ejection of a large fragment of the network is observed in the simulation. This is not a trivial observation as the ejected fragment of the network consists of 168 150 nm long CNTs and has a total mass of ∼50 MDa (not counting the mass of the attached matrix material).

Note that the stability of a network of bundles increases with the length of individual CNTs and the network composed of 150 nm long CNTs is only marginally stable

Fig. 7 (*Continued*)

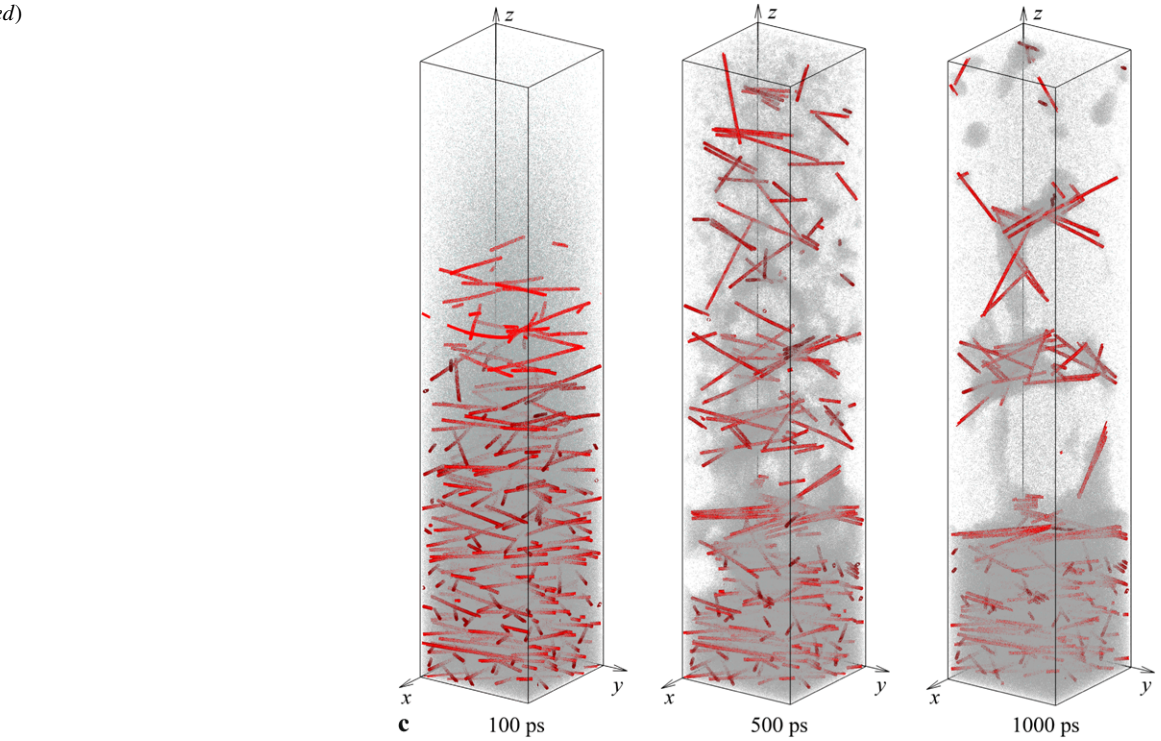

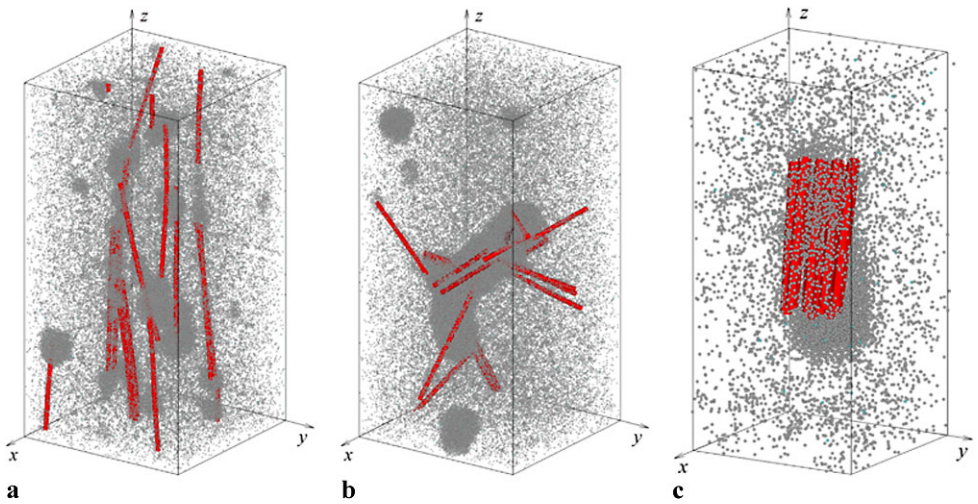

Fig. 8 Snapshots of several typical molecular clusters/droplets and CNT arrangements present in the plume ejected in MAPLE of CNT solutions. Snapshot in (**a**) is taken at 1 ns after the beginning of the laser pulse in a simulation performed for a target loaded with 8 wt.% of 44 nm long CNTs arranged in a *3D random* configuration. Snapshot in (**b**) is taken at 1150 ps after the beginning of the laser pulse in simulations performed for a target loaded with 8 wt.% of 44 nm long CNTs arranged in a *2D random* configuration. Snapshot in (**c**) is taken at 1 ns after the beginning of the laser pulse in a simulation performed for a target loaded with 17 wt.% of 16 nm long CNTs arranged in a *2D random* in configuration. The scale of the snapshot (**c**) is 2.5 times larger than in (**a**) and (**b**). The nanotubes are shown as *red cylinders* and the matrix molecules are shown as *small gray dots*

against decomposition into individual bundles [55]. One can expect that network structures composed of longer CNTs put up stronger resistance to the disintegration and, for short laser pulses and large laser penetration depth, can result in the generation of larger transient pressure in the ablation process mechanically confined by the network. The conditions of the mechanical confinement in this case have some similarity to the ones imposed by collagen fibers and other structural elements of extracellular matrix on the explosive boiling of water-like medium in laser ablation of soft collagenous tissue [73, 85–87]. In the case of more open network structures, shorter laser absorption depth, and/or

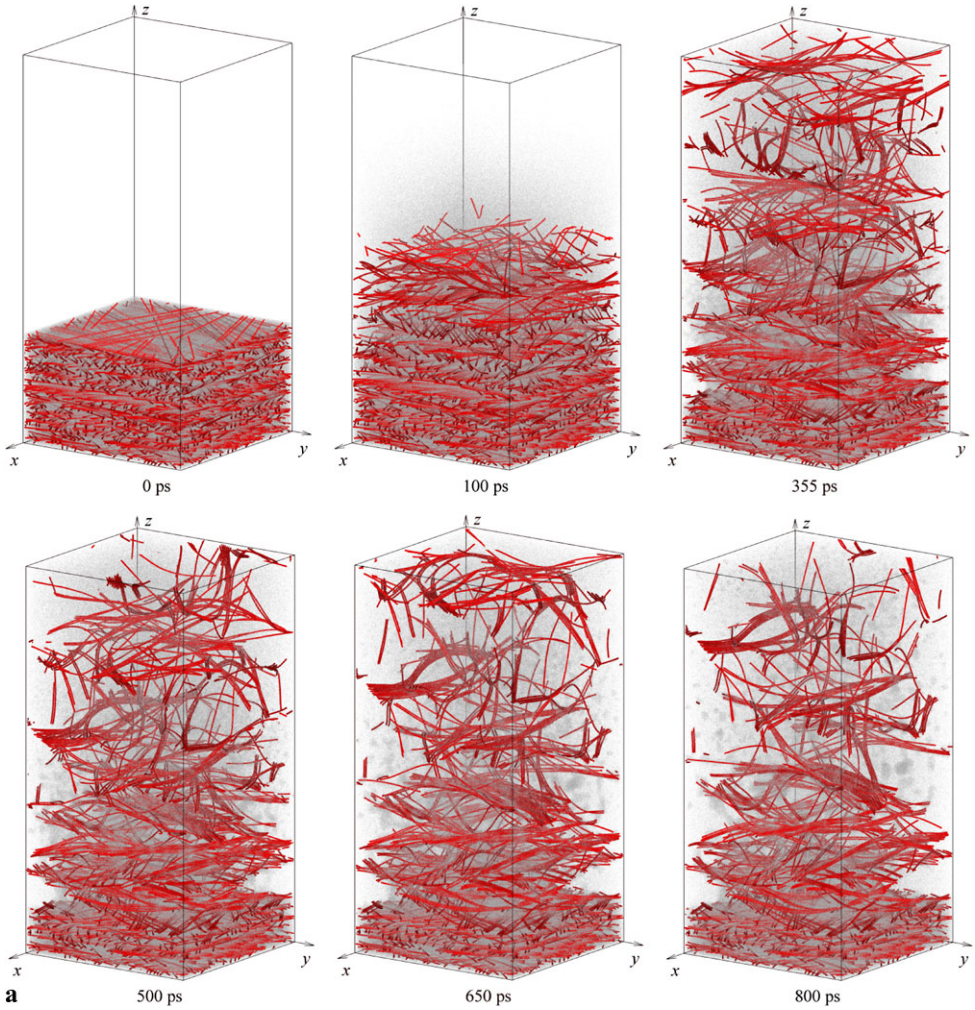

Fig. 9 Snapshots of molecular configurations obtained in large-scale simulations of the ejection of CNTs from MAPLE targets loaded with 17 wt.% of 150 nm long CNTs. The arrangement of the individual nanotubes in the targets is *2D random* in (**a**) and *network of bundles* in (**b**). The nanotubes are shown as *red cylinders* and the matrix molecules are shown as *small gray* dots. Animated sequence of snapshots from the simulations can be found at [76]

longer pulses, the matrix may escape the target leaving behind a skeleton of the CNT network in a matrix-depleted surface region. Direct computational verification of these scenarios, however, is not possible at this time as simulations of larger networks with explicit molecular-level representation of the matrix are beyond the current computational capabilities (the size of the computational cell used in the simulations shown in Fig. 9 is close to the limit of what can be simulated with a parallel code in a reasonable time on a thousand of processors).

In all of the simulations discussed above, the length of the CNTs is comparable or larger than the laser penetration depth. Nevertheless, the individual CNTs and CNT bundles are shown to be entrained by the expanding matrix and ejected from the target, suggesting that large structural elements can be efficiently transported to the substrate in MAPLE deposition of nanocomposite films and coatings. This computational prediction is consistent with experimental observations of MAPLE deposition of clusters/tangles of single-walled CNTs with length of the individual CNTs exceeding the laser penetration depth in the target [46]. For the conditions when the CNTs are much smaller than the laser penetration depth, one can expect the ejection of matrix droplets containing multiple CNTs. The film deposition process in this case is likely to be similar to the one discussed for polymer molecules in Sect. 3 and the distribution of CNTs in the films can be expected to be largely defined by deposition of droplets and rearrangement of the deposited material in the process of matrix vaporization.

5 Summary

Coarse-grained MD simulations of the ejection of polymer molecules and CNTs in MAPLE reveal the mechanistic picture of the matrix-assisted molecular transfer and establish a number of inherent characteristics of the ejection process that have direct implications for the performance of this promising thin film deposition technique. The polymer molecules and nanotubes are found to be ejected only in the ablation regime, when the explosive boiling of the overheated matrix drives the collective ejection of a plume consisting of vapor, molecular clusters, and liquid droplets. The

Fig. 9 (*Continued*)

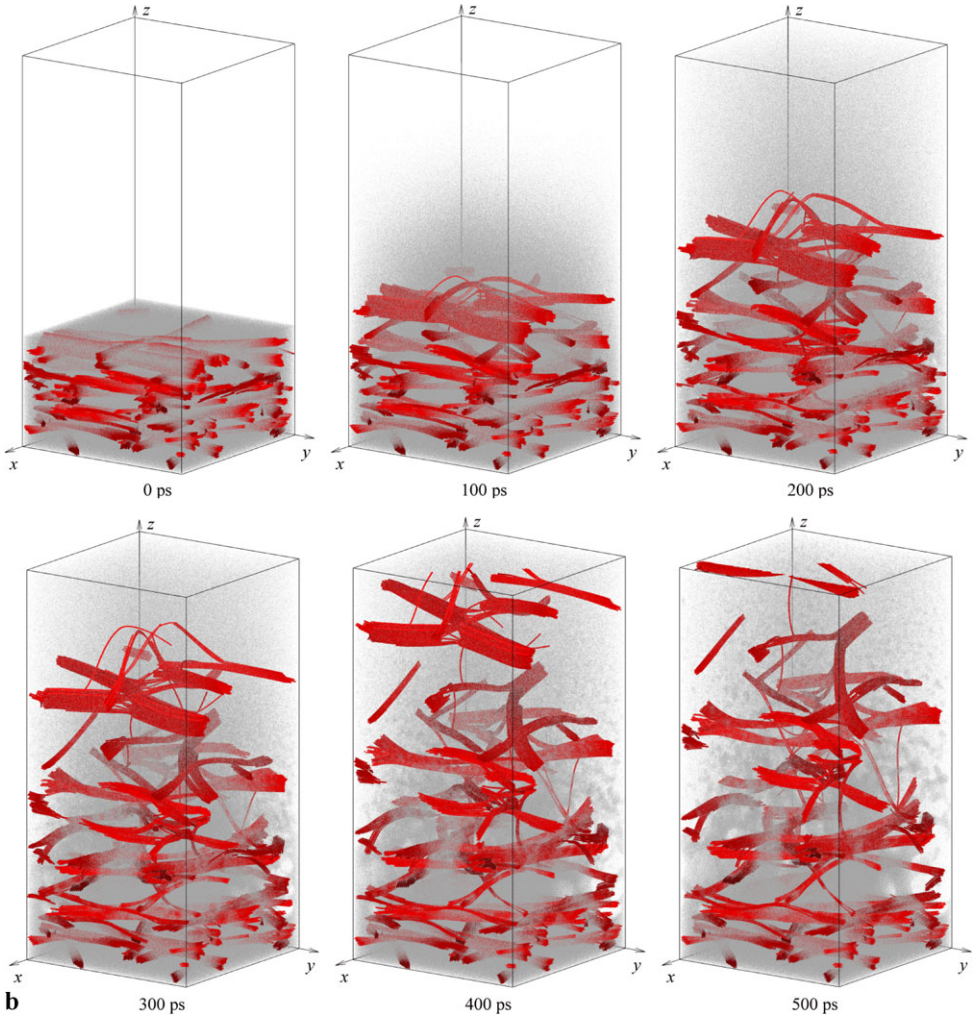

conditions for the onset of the explosive boiling and ablation are defined by the thermodynamic properties of the volatile matrix material and no thermal decomposition of polymer molecules is observed in any of the simulations of MAPLE. In sharp contrast to MAPLE, in a simulation of laser ablation of a polymer target, the dissociation of a large fraction of chemical bonds is observed close to the ablation threshold and no intact molecules survive the ejection process. Thus, the MAPLE technique provides an attractive alternative to PLD when the soft ejection and deposition of polymer molecules without chemical modification and reduction of the molecular weight are required.

The simulations also reveal that polymer molecules are always ejected as parts of large matrix clusters and droplets generated in the process of the explosive disintegration of the overheated matrix. The entanglement of polymer molecules facilitates the formation of intricate elongated viscous droplets that can be related to complex morphologies of polymer films deposited by MAPLE. Since the maximum size of the droplets scales with the laser penetration depth and the size of the polymer features generated by the deposition of droplets is defined by their polymer content, the roughness of the deposited films can, to a certain extent, be reduced by decreasing the laser absorption depth and polymer concentration in the target.

The ability of the MAPLE technique to eject and transfer large structural elements that may be required for deposition of nanostructured films and coatings is demonstrated in simulations performed for MAPLE targets loaded with CNTs. The CNTs with length comparable to or even exceeding the laser penetration depth are found to be efficiently entrained in the expanding matrix plume and lifted off from the target under irradiation conditions that do not cause any chemical damage to polymer molecules. A desired scenario in which the explosive ejection process in MAPLE would disintegrate the CNT bundles formed during the target preparation, leading to an improved dispersion of nanotubes in the deposited films, is not supported by the simulation results. On the contrary, a pronounced tendency of the ejected nanotubes to align along the flow direction of the matrix plume is found to facilitate the bundle formation during the initial stage of the ablation plume expansion. In a simulation of MAPLE per-

formed for a target containing a network of interconnected CNT bundles, a large tangle of CNT bundles is found to be torn out from the continuous network and ejected with the matrix plume, but no signs of any significant splitting and thinning of individual CNT bundles are observed. On the positive side, the survival of large bundles, where the CNTs are held together by relatively weak van der Waals forces, suggests that fragile structural elements or molecular agglomerates with complex secondary structures may be transferred and deposited to the substrate with the MAPLE technique. Finally, we note that the mass of CNT agglomerates (network fragments) ejected in the simulations can be as large as 50 MDa, even though the simulations are performed for a relatively short laser penetration depth of 50 nm. This observation highlights the ability of the MAPLE technique to transfer large macromolecules and structural elements for deposition of biological and nanocomposite films with complex structure and functionality.

Acknowledgements Financial support for this work is provided by AFOSR (Grant FA9550-10-10545) and NSF (Grants CMMI-0800786 and CBET-1033919). Computational support is provided by NCCS at ORNL (project MAT009).

References

1. H.M. Smith, A.F. Turner, Appl. Opt. **4**, 147 (1965)
2. D.B. Chrisey, G.K. Hubler (eds.), *Pulsed Laser Deposition of Thin Films* (Wiley-Interscience, New York, 1994)
3. R. Srinivasan, B. Braren, Chem. Rev. **89**, 1303 (1989)
4. N. Bityurin, B.S. Luk'yanchuk, M.H. Hong, T.C. Chong, Chem. Rev. **103**, 519 (2003)
5. M. Sadoqi, S. Kumar, Y. Yamada, J. Thermophys. Heat Transf. **16**, 193 (2002)
6. M. Prasad, P.P. Conforti, B.J. Garrison, J. Appl. Phys. **101**, 103113 (2007)
7. G.B. Blanchet, Appl. Phys. Lett. **62**, 479 (1993)
8. T. Katoh, Y. Zhang, Appl. Phys. Lett. **68**, 865 (1996)
9. A. Piqué, R.A. McGill, D.B. Chrisey, J. Callahan, T.E. Mlsna, Mater. Res. Soc. Symp. Proc. **526**, 375 (1998)
10. R.A. McGill, R. Chung, D.B. Chrisey, P.C. Dorsey, P. Matthews, A. Pique, T.E. Mlsna, J.I. Stepnowski, IEEET Ultrason. Ferr, **45**, 1370 (1998)
11. A. Piqué, R.A. McGill, D.B. Chrisey, D. Leonhardt, T.E. Mslna, B.J. Spargo, J.H. Callahan, R.W. Vachet, R. Chung, M.A. Bucaro, Thin Solid Films **355/356**, 536 (1999)
12. D.B. Chrisey, A. Piqué, R.A. McGill, J.S. Horwitz, B.R. Ringeisen, D.M. Bubb, P.K. Wu, Chem. Rev. **103**, 553 (2003)
13. J.M. Fitz-Gerald, G. Jennings, R. Johnson, C.L. Fraser, Appl. Phys. A **80**, 1109 (2005)
14. R. Pate, K.R. Lantz, A.D. Stiff-Roberts, IEEE J. Sel. Top. Quant. **14**, 1022 (2008)
15. R. Pate, K.R. Lantz, A.D. Stiff-Roberts, Thin Solid Films **517**, 6798 (2009)
16. D. Adil, N.B. Ukah, R.K. Gupta, K. Ghosh, S. Guha, Synth. Met. **160**, 2501 (2010)
17. B.R. Ringeisen, J. Callahan, P.K. Wu, A. Piqué, B. Spargo, R.A. McGill, M. Bucaro, H. Kim, D.M. Bubb, D.B. Chrisey, Langmuir **17**, 3472 (2001)
18. L. Stamatin, R. Cristescu, G. Socol, A. Moldovan, D. Mihaiescu, I. Stamatin, I.N. Mihailescu, D.B. Chrisey, Appl. Surf. Sci. **248**, 422 (2005)
19. R. Cristescu, D. Mihaiescu, G. Socol, I. Stamatin, I.N. Mihailescu, D.B. Chrisey, Appl. Phys. A **79**, 1023 (2004)
20. A. Purice, J. Schou, P. Kingshott, N. Pryds, M. Dinescu, Appl. Surf. Sci. **253**, 6451 (2007)
21. A. Purice, J. Schou, P. Kingshott, M. Dinescu, Chem. Phys. Lett. **435**, 350 (2007)
22. P.K. Wu, B.R. Ringeisen, J. Callahan, M. Brooks, D.M. Bubb, H.D. Wu, A. Piqué, B. Spargo, R.A. McGill, D.B. Chrisey, Thin Solid Films **398–399**, 607 (2001)
23. P.K. Wu, B.R. Ringeisen, D.B. Krizman, C.G. Frondoza, M. Brooks, D.M. Bubb, R.C.Y. Auyeung, A. Piqué, B. Spargo, R.A. McGill, D.B. Chrisey, Rev. Sci. Instrum. **74**, 2546 (2003)
24. T.M. Patz, A. Doraiswamy, R.J. Narayan, N. Menegazzo, C. Kranz, B. Mizaikoff, Y. Zhong, R. Bellamkonda, J.D. Bumgardner, S.H. Elder, X.F. Walboomers, R. Modi, D.B. Chrisey, Mater. Sci. Eng., C, Biomim. Mater., Sens. Syst. **27**, 514 (2007)
25. A. Gutiérrez-Llorente, G. Horowitz, R. Pérez-Casero, J. Perriére, J.L. Fave, A. Yassar, C. Sant, Org. Electron. **5**, 29 (2004)
26. R.K. Gupta, K. Ghosh, P.K. Kahol, J. Yoon, S. Guha, Appl. Surf. Sci. **254**, 7069 (2008)
27. A. Gutiérrez-Llorente, R. Pérez-Casero, B. Pajot, J. Roussel, R.M. Defourneau, D. Defourneau, J.L. Fave, E. Millon, J. Perriere, Appl. Phys. A **77**, 785 (2003)
28. R. Fryček, M. Jelínek, T. Kocourek, P. Fitl, M. Vrňata, V. Myslík, M. Vrbová, Thin Solid Films **495**, 308 (2006)
29. A.T. Sellinger, E.M. Leveugle, K. Gogick, L.V. Zhigilei, J.M. Fitz-Gerald, J. Vac. Sci. Technol., A, Vac. Surf. Films **24**, 1618 (2006)
30. A.T. Sellinger, E. Leveugle, K. Gogick, G. Peman, L.V. Zhigilei, J.M. Fitz-Gerald, J. Phys. Conf. Ser. **59**, 314 (2007)
31. A.L. Mercado, C.E. Allmond, J.G. Hoekstra, J.M. Fitz-Gerald, Appl. Phys. A **81**, 591 (2005)
32. D.M. Bubb, M. Papantonakis, B. Collins, E. Brookes, J. Wood, U. Gurudas, Chem. Phys. Lett. **448**, 194 (2007)
33. D.M. Bubb, J. Corgan, S.Y. Yi, M. Khan, L. Hughes, U. Gurudas, M. Papantonakis, R.A. McGill, Appl. Phys. A **100**, 523 (2010)
34. A.P. Caricato, M. Anni, M.G. Manera, M. Martino, R. Rella, F. Romano, T. Tunno, D. Valerini, Appl. Surf. Sci. **255**, 9659 (2009)
35. A.P. Caricato, G. Leggieri, M. Martino, A. Vantaggiato, D. Valerini, A. Cretì, M. Lomascolo, M.G. Manera, R. Rella, M. Anni, Appl. Phys. A **101**, 759 (2010)
36. R. Pate, A.D. Stiff-Roberts, Chem. Phys. Lett. **477**, 406 (2009)
37. K. Rodrigo, P. Czuba, B. Toftmann, J. Schou, R. Pedrys, Appl. Surf. Sci. **252**, 4824 (2006)
38. V. Califano, F. Bloisi, L.R.M. Vicari, P. Colombi, E. Bontempi, L.E. Depero, Appl. Surf. Sci. **254**, 7143 (2008)
39. A. Stanculescu, L. Vacareanu, M. Grigoras, M. Socol, G. Socol, F. Stanculescu, N. Preda, E. Matei, I. Ionita, M. Girtan, I.N. Mihailescu, Appl. Surf. Sci. **257**, 5298 (2011)
40. E. Leveugle, L.V. Zhigilei, J. Appl. Phys. **102**, 074914 (2007)
41. E. Leveugle, A. Sellinger, J.M. Fitz-Gerald, L.V. Zhigilei, Phys. Rev. Lett. **98**, 216101 (2007)
42. A. Sellinger, E. Leveugle, J.M. Fitz-Gerald, L.V. Zhigilei, Appl. Phys. A **92**, 821 (2008)
43. A. Luches, A.P. Caricato, Appl. Phys. B (2011, in press). doi:10.1007/s00340-011-4519-y
44. L.V. Zhigilei, B.J. Garrison, J. Appl. Phys. **88**, 1281 (2000)
45. L.V. Zhigilei, Appl. Phys. A **76**, 339 (2003)
46. A.T. Sellinger, A.H. Martin, J.M. Fitz-Gerald, Thin Solid Films **516**, 6033 (2008)
47. A.P. Caricato, S. Capone, G. Ciccarella, M. Martino, R. Rella, F. Romano, J. Spadavecchia, A. Taurino, T. Tunno, D. Valerini, Appl. Surf. Sci. **253**, 7937 (2007)
48. A.P. Caricato, A. Luches, R. Rella, Sensors **9**, 2682 (2009)

49. P.K. Wu, J. Fitz-Gerald, A. Piqué, D.B. Chrisey, R.A. McGill, Mater. Res. Soc. Symp. Proc. **617**, J2.3.1 (2000)
50. L.V. Zhigilei, P.B.S. Kodali, B.J. Garrison, J. Phys. Chem. B **101**, 2028 (1997)
51. E.A. Colbourn (ed.), *Computer Simulation of Polymers* (Longman, Harlow, 1994)
52. A.I. Kitaigorodsky, *Molecular Crystals and Molecules* (Academic Press, New York, 1993)
53. L.V. Zhigilei, C. Wei, D. Srivastava, Phys. Rev. B **71**, 165417 (2005)
54. A.N. Volkov, L.V. Zhigilei, J. Phys. Chem. C **114**, 5513 (2010)
55. A.N. Volkov, L.V. Zhigilei, ACS Nano **4**, 6187 (2010)
56. D.W. Brenner, O.A. Shenderova, J.A. Harrison, S.J. Stuart, B. Ni, S.B. Sinnott, J. Phys., Condens. Matter **14**, 783 (2002)
57. A.N. Volkov, K.R. Simov, L.V. Zhigilei, in *Proceedings of the ASME International Mechanical Engineering Congress and Exposition, ASME paper IMECE2008-68021* (ASME, New York, 2008)
58. S.J. Stuart, A.B. Tutein, J.A. Harrison, J. Chem. Phys. **112**, 6472 (2000)
59. A.N. Volkov, L.V. Zhigilei, in *Computational Fluid Dynamics 2010*, ed. by A. Kuzmin (Springer, Berlin, 2011), pp. 823–831
60. M. Grujicic, G. Cao, W.N. Roy, J. Mater. Sci. **39**, 2315 (2004)
61. L.A. Girifalco, M. Kodak, R.S. Lee, Phys. Rev. B **62**, 13104 (2000)
62. L.V. Zhigilei, B.J. Garrison, Mater. Res. Soc. Symp. Proc. **538**, 491 (1999)
63. J. Liu, A.G. Rinzler, H. Dai, J.H. Hafner, R.K. Bradley, P.J. Boul, A. Lu, T. Iverson, K. Shelimov, C.B. Huffman, F. Rodriguez-Macias, Y.-S. Shon, T.R. Lee, D.T. Colbert, R.E. Smalley, Science **280**, 1253 (1998)
64. A.N. Volkov, K.R. Simov, L.V. Zhigilei, in *Proceedings of the 47th AIAA Aerospace Sciences Meeting, AIAA paper 2009-1544* (AIAA, Reston, 2009)
65. A. Thess, R. Lee, P. Nikolaev, H. Dai, P. Petit, J. Robert, C. Xu, Y.H. Lee, S.G. Kim, A.G. Rinzler, D.T. Colbert, G.E. Scuseria, D. Tománek, J.E. Fischer, R.E. Smalley, Science **273**, 483 (1996)
66. S. Wang, Z. Liang, B. Wang, C. Zhang, Adv. Mater. **19**, 1257 (2007)
67. R. Shvartzman-Cohen, E. Nativ-Roth, E. Baskaran, Y. Levi-Kalisman, I. Szleifer, R. Yerushalmi-Rozen, J. Am. Chem. Soc. **126**, 14850 (2004)
68. D.S. Kim, D. Nepal, K.E. Geckeler, Small **1**, 1117 (2005)
69. J. Gou, Polym. Int. **55**, 1283 (2006)
70. Z. Wang, Z. Liang, B. Wang, C. Zhang, L. Kramer, Composites, Part A, Appl. Sci. Manuf. **35**, 1225 (2004)
71. Y. Murakami, E. Einarsson, T. Edamura, S. Maruyama, Phys. Rev. Lett. **94**, 087402 (2005)
72. L.V. Zhigilei, E. Leveugle, B.J. Garrison, Y.G. Yingling, M.I. Zeifman, Chem. Rev. **103**, 321 (2003)
73. A. Vogel, V. Venugopalan, Chem. Rev. **103**, 577 (2003)
74. A.A. Oraevsky, S.L. Jacques, F.K. Tittel, J. Appl. Phys. **78**, 1281 (1995)
75. G. Paltauf, P.E. Dyer, Chem. Rev. **103**, 487 (2003)
76. Animated sequences of snapshots from the simulations illustrated in Figs. 3, 7, and 9 can be found at http://www.faculty.virginia.edu/CompMat/maple/
77. L.V. Zhigilei, P.B.S. Kodali, B.J. Garrison, Chem. Phys. Lett. **276**, 269 (1997)
78. B.J. Garrison, J.E. Itina, L.V. Zhigilei, Phys. Rev. E **68**, 041501 (2003)
79. A. Miotello, R. Kelly, Appl. Phys. A **69**, S67 (1999)
80. R. Kelly, A. Miotello, J. Appl. Phys. **87**, 3177 (2000)
81. N.M. Bulgakova, A.V. Bulgakov, Appl. Phys. A **73**, 199 (2001)
82. L.V. Zhigilei, Z. Lin, D.S. Ivanov, J. Phys. Chem. C **113**, 11892 (2009)
83. E. Leveugle, L.V. Zhigilei, A. Sellinger, J.M. Fitz-Gerald, Appl. Surf. Sci. **253**, 6456 (2007)
84. E. Leveugle, L.V. Zhigilei, A. Sellinger, J.M. Fitz-Gerald, J. Phys. Conf. Ser. **59**, 126 (2007)
85. N.P. Furzikov, Sov. J. Quantum Electron. **21**, 222 (1991)
86. M.S. Kitai, V.L. Popkov, V.A. Semchishen, A.A. Kharizov, IEEE J. Quantum Electron. **27**, 302 (1991)
87. I. Apitz, A. Vogel, Appl. Phys. A **81**, 329 (2005)